The Journal of Engineering

*The 9th International Conference on Power Electronics, Machines and Drives (PEMD 2018)*

IET Journals
The Institution of Engineering and Technology

# TC48: A low-cost 48 V integrated drive for mild hybrid electric vehicles

eISSN 2051-3305
Received on 26th June 2018
Accepted on 30th July 2018
doi: 10.1049/joe.2018.8260
www.ietdl.org

*Dave Winterborne[1] ✉, Muez Shiref[1], Stuart Snow[2], Volker Pickert[1]*

[1]*School of Engineering, Newcastle University, Newcastle-upon-Tyne, UK*
[2]*RDM Ltd., Coventry, UK*
✉ *E-mail: dave.winterborne@ncl.ac.uk*

**Abstract:** The TC48 drive is a low-cost, low-voltage integrated motor-drive solution suitable for mild hybrid electric vehicles, off-highway traction, and any application where a compact, highly torque-dense machine is required. Low-voltage solutions for electric vehicles are attractive to manufacturers due to lower insulation requirements, and hence lower cost. The package is based on a six-phase switched reluctance machine, which uses a novel stator topology and unique winding design to achieve high torque density. The power electronics converter hardware is integrated into the motor housing, giving a physically, electrically, and thermally optimised solution. The complete package has been designed to be suitable for manufacturing in high volumes. This study describes the electromagnetic design of the motor, the mechanical innovations used to physically realise this design, and the cooling system which makes the high power density possible. The integration of the power electronics and their control is also discussed. The project is the result of collaboration between Newcastle and Loughbosrough Universities, RDM Ltd., Productiv, Infineon, Tata Steel, and Libralato.

## 1 Introduction

Recent years have seen increasing interest in low-voltage (<60 V) traction systems for mild hybrid electric vehicles [1–5]. Many electric vehicles use higher voltages – typically between 300 and 800 V DC [6] – to obtain greater efficiencies from the easier design of faster, more power dense, machines, and reduce losses due to lower currents [7]. However, the low voltage has advantages too, particularly in micro and mild hybrid applications where power levels are lower. Such solutions are easier to integrate into existing vehicle platforms. The lower voltage is inherently safer and reduces the requirement for insulation, decreasing cost, and weight [8]. Research has found that low-voltage power electronic converters themselves are cost-neutral compared with high-voltage systems, as the lower voltage rating is offset by higher device count, but the requirement for isolation between the traction supply and the auxiliary supply (typically 12 V) is removed [9].

Perhaps most telling is the number of high-profile international industrially focussed conferences and expos dedicated to, or with a heavy emphasis on, 48 V electric vehicles in both Europe and America. Examples include the Electric and Hybrid Vehicle Technology Expo, and the International Conference on Automotive 48 V Power Supply Systems, both featuring speakers from major carmakers and tier 1 suppliers.

Motors that do not contain permanent magnets have also proved increasingly popular with original equipment manufacturer (OEMs) as the cost of rare-earth magnet materials is particularly volatile [10, 11]. Switched reluctance machines, in particular, are well suited to automotive traction applications due to their low cost, rugged construction, and wide constant power speed range [12–14].

Another recent trend in electric drives, particularly in the automotive sector, is the integration of the electric machine, and power and control electronics into a single package. This results in higher torque density, reduced size and weight due to less housing and connectors, and higher efficiency due to reduced losses. Reducing the distance between the power electronics and motor windings is particularly important when using high currents as in this low-voltage drive.

## 2 Motor design

### 2.1 Topology and winding design

Achieving the target output power of 21 kW in a 48 V system with a maximum speed of 7500 rpm necessitates high currents within the machine and this has a profound effect on the design choices made.

Increasing the number of stator poles enables the current, and hence resistive losses (which dominate this system) [15], to be distributed more easily around the machine and reduces torque ripple [16]. The trade-off is the decrease in tooth width, which makes saturation in the core harder to avoid, increases the required manufacturing accuracy, makes assembly more difficult, and increases the number of interconnections [17]. The switching frequency needed for high fidelity control is also increased. As a compromise, a 6-phase 12–10 topology was chosen, with two parallel coils making up each phase.

The low-voltage dictates a low turn number, and so placement of the coil conductors within the slot becomes important. The high currents make reducing the resistance, and hence increasing the fill factor, a priority. Hence, a 10-turn pre-formed coil design is used, with a $5 \times 2$ conductor layout, as shown in Fig. 1. The four-part former, which allows compression of the coil radially and circumferentially, is shown in Fig. 2. A coil with a high fill factor also enables effective heat transfer to the stator laminations and ultimately the cooling system [18].

The machine is designed for a maximum speed of 7500 rpm, but due to the high pole number, the fundamental frequency is still relatively high at 1.25 kHz, and so a type 1 Litz wire consisting of seven strands is used to reduce AC losses and help spread the loss more evenly throughout the conductor.

### 2.2 Stator design

In order to achieve high current density in the stator windings, it is desirable to pre-form the coils prior to assembly onto the iron core, in order to achieve the maximum copper fill factor possible in the slot [19]. However, this introduces constraints for the geometry of the core laminations and the coil cross-section. To ensure that both the coil and core profile are optimal, a segmented stator design has been used.

Segmented stator topologies have previously been used for fault-tolerance [20] and manufacturing reasons [21, 22].

**Fig. 1** *Pre-formed coil*

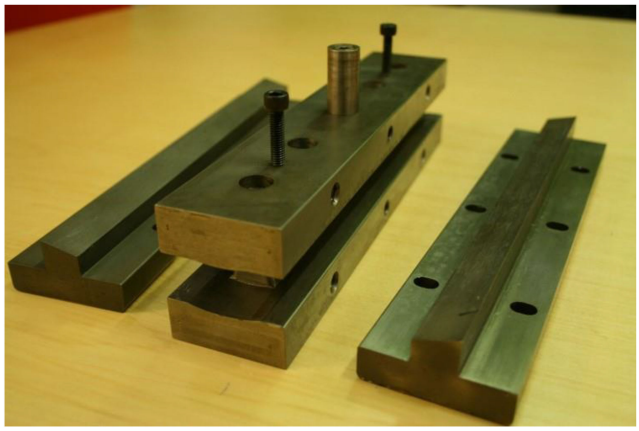

**Fig. 2** *Coil former*

## 3 Power electronics integration

To maximise the torque at high speeds, the achievable rate of change of current must be high. Given the relatively limited voltage, it is important to minimise the inductance of the windings. Therefore, the conductors between the power electronic converter and motor windings must be kept as short as possible to keep the self-inductance of the coil as low as possible.

Furthermore, the high current dictates that the resistance of the conductors should be kept as low as possible, which reinforces the need for the path between the power devices and coils to be as short as possible.

The power electronic devices are implemented on 12 identical power modules, mounted 2 per face on the hexagonal water jacket of the motor, as shown in Fig. 3. This results in very short, symmetrical connections between the motor windings and the power electronics. Making each connection of the same length means that all the coils will have similar electrical properties and this helps to simplify control.

The drive topology is nominally a six-phase asymmetric half-bridge, though the diodes are implemented using the same metal-oxide-semiconductor field-effect transistors (MOSFETs) as the switching devices (i.e. each coil is driven from a full bridge), resulting in a simplified design where all the power devices are the same part. Each device is implemented using three parallel MOSFETs. The low voltage makes the use of MOSFETs preferable due to lower switching losses. The positive temperature coefficient of their on-state resistance [23] also means they can be paralleled with ease, and hence the total loss reduced and more widely distributed on the printed circuit board (PCB).

The distributed DC link capacitance is implemented on these boards, keeping the capacitors as close as possible to the power devices. The short paths and the use of low equivalent series resistance (ESR) ceramic capacitors mean that the overall volume of the capacitance is minimised.

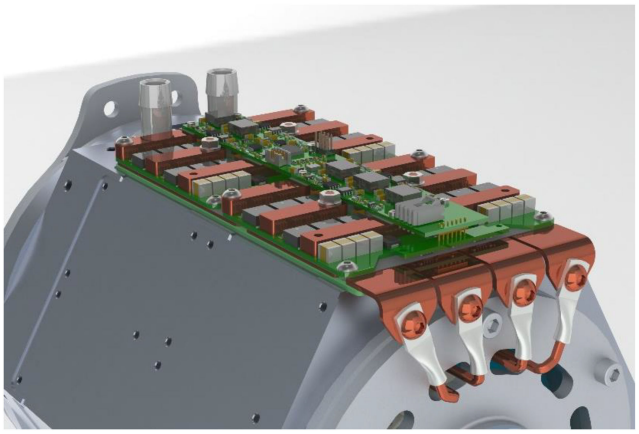

**Fig. 3** *Power modules integrated onto water jacket (one side populated)*

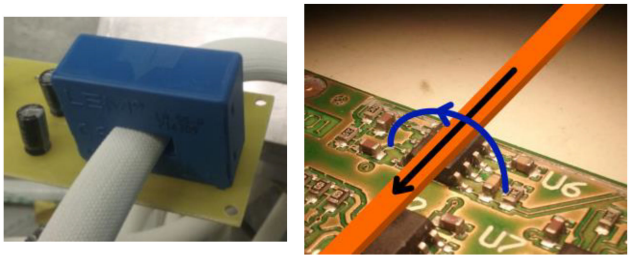

*a* *b*

**Fig. 4** *Hall-effect current sensors*
***(a)*** With the magnetic core, ***(b)*** Without the magnetic core

### 3.1 Controller architecture

Each face also has one logic board containing a local controller, current- and temperature-sensing devices, and gate drives. These are responsible for low-level current control of the devices on that face and are controlled by a central controller via a controller area network (CAN) interface.

### 3.2 Current sensing

Owing to the close physical integration of the power electronics and motor, the implementation of phase current sensing for the controller feedback loop presents something of a challenge.

Conventional Hall-effect sensors, as shown in Fig. 4*a*, usually feature a ferrite core which surrounds the conductor under measurement and concentrates the field through the Hall-effect element. This makes the sensor largely insensitive to magnetic fields other than that created by the current flowing through the core in the measured conductor but results in a large package – ~13 $cm^3$ for a 300 A device required for this drive [24].

Provided care is used in the electromagnetic design, a surface mount Hall-effect transducer with no external core, as shown in Fig. 4*b*, with an example conductor location and the current flow and magnetic field indicated, can be used. This must be placed in an appropriate location and orientation with respect to the conductor to be measured and taking into account other magnetic fields in the drive. The measurement is also sensitive to the separation between the conductor and the transducer, so this must be closely controlled and the transducers should be individually calibrated.

As no external core is used to concentrate the flux produced by the measured conductor, the Hall-effect element must have greater sensitivity, and it will be more sensitive to stray fields as well as to the field of interest. The transducers are located on top of each phase distribution bar (described in Section 3.3), directly underneath the sub-controller PCBs and so the main source of stray flux is the machine winding.

One location used is directly above the end winding, and so the main component of the stray field in the region of the sensor is parallel to the axis of the machine, orthogonal to the flux produced by the current in the phase distribution bar. Therefore, it does not

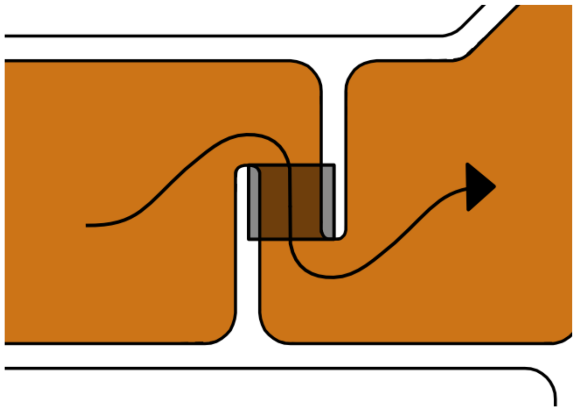

**Fig. 5** *Slots in bus bar to guide current into appropriate direction to avoid interference from stray fields [25]*

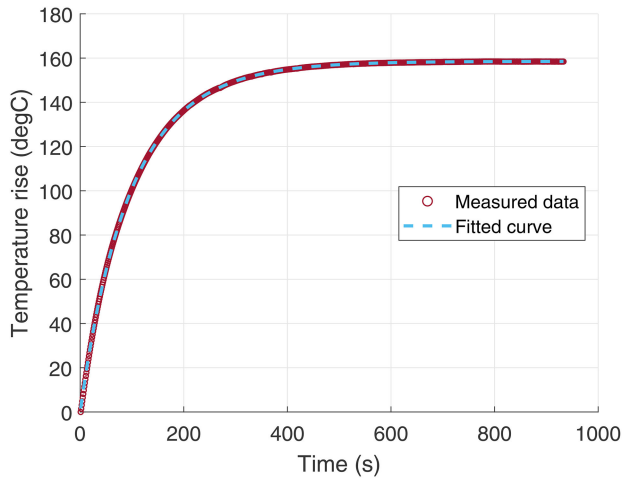


**Fig. 6** *Thermal testing results and the fitted curve*

affect the current measurement with the Hall-effect element in its 'natural' orientation. The material is removed from the phase distribution bar to give a narrow section where the current sensor is located, in order to concentrate the magnetic field on the sensor. Experimentation has revealed that this does not have a significant impact on the heating of the phase distribution bar.

The other location used is above the main part of the winding, where the currents in the windings and phase distribution bar are parallel, and hence, their magnetic fields are coplanar. To avoid interference, the bus bar is designed with slots to guide the flux through a 'neck', orthogonal to the motor axis, where the sensor is located, as shown in Fig. 5. Thus, the Hall-effect element is sensitive to the flux produced by the current in the phase distribution bar, but not the motor winding.

The small size and cost of the current sensor permit one to be used per phase distribution bar in the prototype machine: two per coil, four per phase. This allows not only the active balancing of current between coils in the same phase, but also provides redundancy for current measurement in the same phase to mitigate against any remaining stray field issues, device failures, or other issues.

### *3.3 Thermal management*

Due to the high current density in the machine windings, cooling must be carefully considered. The machine and power electronics share a common cooling system. A conventional water jacket arrangement is used to cool the machine, but the outer surface is a hexagonal prism onto which the power electronics are mounted.

The conductors between the motor windings and power electronics, while short, carry very high currents and therefore good thermal contact to the coolant must be maintained wherever possible to avoid localised heating. An arrangement of copper bus bars soldered to an insulated metal substrate (IMS) between the water jacket and PCBs is used to maintain good thermal contact between the conductors and the cooled surface while insulating electrically. This also forms the thermal path between the power electronics and water jacket.

This phase distribution arrangement is manufactured using standard processes: laser-cut or stamped copper sheet is reflow soldered to a standard IMS. Copper studs are welded onto the bus bars and carry the current to the phase bars on the power module above.

The wide, thin profile of the copper bars provides a large cross-sectional area, and hence, low resistance while utilising the space effectively to keep the outer diameter of the drive package low. It also reduces skin effect and proximity loss at higher frequencies.

Combining the cooling of power electronics and machine results in a solution which is more easily integrated into an existing vehicle design or other application. Only a single coolant supply and return are required.

## 4 Simulation and practical testing

### *4.1 Thermal testing*

An indication of the thermal performance of the machine was obtained by supplying the current equivalent to the peak power to a single coil. Since the drive is rated for 600 A peak current per phase, 300 A is the peak coil current, and 150 A DC is chosen to represent this, assuming the waveform approximates a square wave with a 50% duty cycle. This approximation neglects iron loss, which is relatively small owing to the high current causing resistive loss to dominate.

The resulting temperature rise with 15 l/min coolant flow rate at 20°C inlet temperature is shown in Fig. 6.

An exponential curve with two components, representing the thermal impedance of the coil and the core/housing, is fitted to the experimental data. The general form is

$$\Delta T = T_c(1 - \mathrm{e}^{-t/\tau_c}) + T_h(1 - \mathrm{e}^{-t/\tau_c}) \quad (1)$$

The parameters for this fit, giving an $R^2$ value of 0.9999, are

$T_c = 33.92$°C
$\tau_c = 58.62$ s
$T_h = 124.6$°C
$\tau_h = 112.8$ s

This model allows the temperature and rise time for any given power loss to be calculated.

### *4.2 Static testing*

The machine was designed and simulated using the finite element (FE) method in Infolytica MagNet. Once constructed, the machine was subjected to static torque and 'psi-I' tests to assess its performance and compare with the simulation. Together the characteristics produced by these tests indicate the torque capability of the machine and can be used to determine the requirements of the converter.

The static torque characteristic was found by supplying a single phase with DC in steps of 50 A up to 600 A with the rotor locked in position using a rotary table. The test was repeated at intervals of 10° electrical (1° mechanical for this 10-pole machine). The torque was measured using a torque transducer, which measures the displacement of a shaft of known length and stiffness. An early implementation of the prototype machine (with cylindrical housing) is shown on the static test rig in Fig. 7.

The characteristics are shown in Fig. 8 compared with the 600 A simulated characteristic. The simulated results are generated from a 2D FE model which does not model end-leakage inductance and therefore indicates a slightly higher torque than the constructed machine.

It must also be noted that the unaligned position does not appear to lie exactly halfway between the two aligned positions in the test

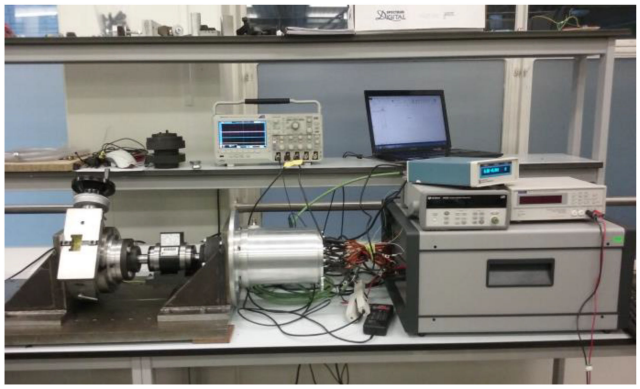

**Fig. 7** *Prototype machine on the static test rig*

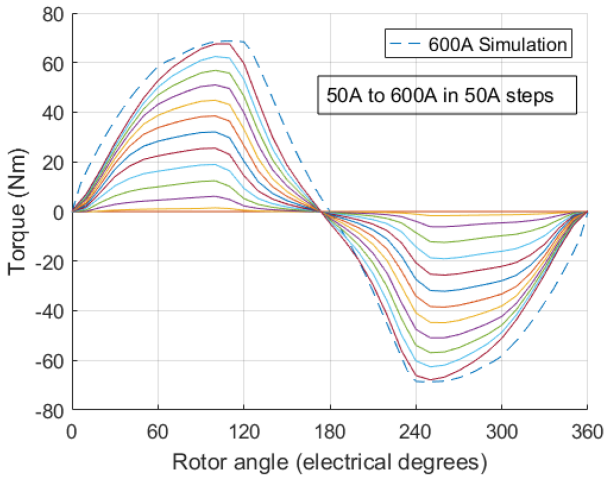


**Fig. 8** *Static torque characteristics – measurement and simulation*

data. A possible cause of this is physical hysteresis in the torque transducer or rotary table.

### *4.3 Drive performance*

The results from the static testing presented in the previous section were used in a model of the complete drive to predict overall performance. This model is implemented in MATLAB Simulink, with the converter circuit modelled using PLECS. Each phase of the machine is represented by a lookup table – based on the measured psi-I characteristics – giving the current according to the applied phase voltage (integrated to find the flux and taking into account the phase resistance), and a lookup table giving the torque for this current, based on the measured static torque characteristic. One limitation of this model is that mutual flux between phases is not modelled.

The controller uses the psi-I data, re-interpreted to give a flux demand to generate a square current waveform, with a deadbeat flux controller [26, 27]. More advanced torque-sharing functions, based on this approach, can be used to reduce torque ripple [28, 29]. The resultant voltage is applied with a conventional pulse width modulation scheme operating at 20 kHz.

The model allows the conduction angle (the interval for which each phase conducts current) and advance angle (the interval before the aligned position at which the phase begins to conduct) to be varied. These parameters are iterated at various speeds throughout the operating range to find the values which produce the highest mean torque over an electrical cycle. A script is used to perform a smart traversal of the conduction-advance angle plane, ensuring that the global maximum is correctly identified without excessive simulation runs. An example of the results of this optimisation at 1750 rpm is shown in Fig. 9.

The complete torque–speed curve produced from the drive simulation with the optimum angle control parameters is shown in Fig. 10 along with the specification torque–speed curve for comparison.

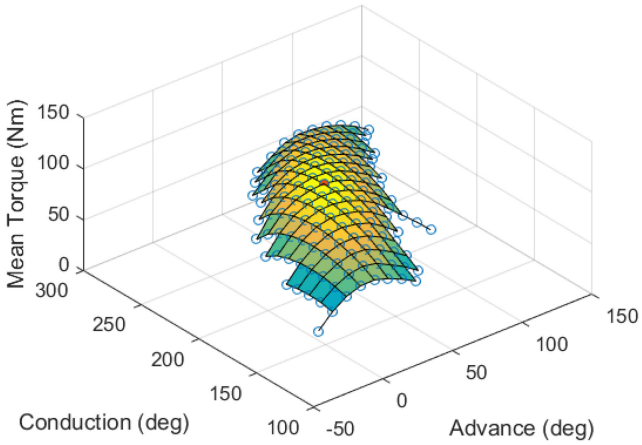


**Fig. 9** *Results of search for optimum advance and conduction angle at 1750 rpm*

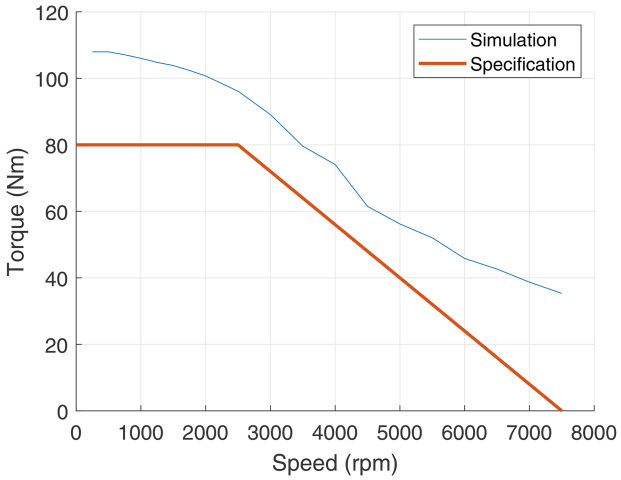


**Fig. 10** *Torque–speed curve produced by drive simulation*

This characteristic represents the maximum torque that can be produced for each speed using the rated current. It does not take into account the thermal limitations of the machine but indicates the limits of short duration performance.

It also does not consider other objectives such as efficiency or torque ripple minimisation.

## 5 Conclusions

The TC48 project has demonstrated a viable design for an integrated switched reluctance drive, achieving high torque density and a compact package within the design space envelope.

This has been made possible by the careful design of each aspect of the drive and the package as a whole. While dynamic experimental testing is yet to take place, the simulation of the drive and static testing of the constructed prototype show that the performance of the drive meets the specification.

While designed as an automotive traction motor for mild hybridisation, the complete unit also represents an attractive proposition for full electrification of a small road vehicle or a variety of off-highway applications such as materials handling.

## 6 Acknowledgments

The authors gratefully acknowledge Innovate UK as the source of funding which made this research possible.

## 7 References

[1] Ha, S.: 'Power distribution control algorithm for fuel economy optimization of 48 V mild hybrid vehicle'. Int. Conf. on Modeling and Applied Simulation, Barcelona, Spain, 2017

[2] Abdellahi, A., Khaleghi Rahimian, S., Blizanac, B., *et al.*: 'Exploring the opportunity space for high-power li-ion batteries in next-generation 48 V mild

hybrid electric vehicles'. WCX™ 17: SAE World Congress Experience, Detroit, MI, USA, March 2017
[3] Naidu, A., Brittle, P., Ma, X., *et al.*: 'Integrated systems engineering approach for incremental 48Volt hybrid technology introduction'. SAE Technical Paper, 2017
[4] Liu, Z., Onori, S., Ivanco, A.: 'Synthesis and experimental validation of battery aging test profiles based on real-world duty cycles for 48-V mild hybrid vehicles'. *IEEE Trans. Veh. Technol.*, 2017, **66**, (10), pp. 8702–8709
[5] Sreedhar, S., Siegel, J.B., Choi, S.: 'Topology comparison for 48 V battery-supercapacitor hybrid energy storage system', *IFAC-PapersOnLine*, 2017, **50**, (1), pp. 4733–4738
[6] ZVEI: 'German electrical and electronic manufacturers' association', Voltage Classes for Electric Mobility, 2013
[7] Bao, J., Boynov, K., Paulides, J.J.H., *et al.*: 'Comparison of 48 V rare-earth-free reluctance traction motor drives for mild hybrid powertrain'. IEEE Vehicle Power and Propulsion Conf. (VPPC), Hangzhou, China, 2016
[8] Bachheibl, F., Gerling, D.: 'High-current, low-voltage power net'. IEEE Int. Electric Vehicle Conf. (IEVC), Florence, Italy, 2014
[9] Gerling, D., Zeljkovic, S., Vuletic, R.: 'An applicability study of LV battery on-board chargers for high power EVs'. IEEE Int. Electric Vehicle Conf. (IEVC), Florence, Italy, 2014
[10] Bramerdorfer, G., Cavagnino, A., Vaschetto, S.: 'Cost-optimal machine designs fulfilling efficiency requirements: A comparison of IMs and PMSMs'. IEEE Int. Electric Machines and Drives Conf. (IEMDC), Miami, FL, USA, 2017
[11] Chen, L., Hopkinson, D., Wang, J., *et al.*: 'Reduced dysprosium permanent magnets and their applications in electric vehicle traction motors', *IEEE Trans. Magn.*, 2015, **51**, (11), pp. 1–4
[12] Jin, Y., Bilgin, B., Emadi, A.: 'Comparative evaluation of power converters for 6/4 and 6/10 switched reluctance machines'. IEEE Transportation Electrification Conf. and Expo (ITEC), Dearborn, MI, USA, 2012
[13] Wu, W., Lovatt, H.C., Dunlop, J.B.: 'Optimisation of switched reluctance motors for hybrid electric vehicles'. Int. Conf. on Power Electronics, Machines and Drives (Conf. Publ. No. 487), Santa Fe, NM, USA, 2002
[14] Yildirim, M., Polat, M., Kürüm, H.: 'A survey on comparison of electric motor types and drives used for electric vehicles'. 2014 16th Int. Power Electronics and Motion Control Conf. and Exposition, Antalya, Turkey, 2014
[15] Manyage, M.J., Pillay, P.: 'Low voltage high current PM traction motor design using recent core loss results'. IEEE Industry Applications Annual Meeting, New Orleans, LA, USA, 2007
[16] Anwar, M.N., Husain, I., Radun, A.V.: 'A comprehensive design methodology for switched reluctance machines', *IEEE Trans. Ind. Appl.*, 2001, **37**, (6), pp. 1684–1692
[17] Bilgin, B., Krishnamurthy, M.: 'An FEA/MATLAB based machine design tool for switched reluctance motors'. IEEE Vehicle Power and Propulsion Conf., Chicago, IL, USA, 2011
[18] Nategh, S., Krings, A., Wallmark, O., *et al.*: 'Evaluation of impregnation materials for thermal management of liquid-cooled electric machines', *IEEE Trans. Ind. Electron.*, 2014, **61**, (11), pp. 5956–5965
[19] Jack, A.G., Mecrow, B.C., Dickinson, P.G., *et al.*: 'Permanent magnet machines with powdered iron cores and pre-pressed windings'. Conf. Record of the IEEE Industry Applications Conf. Thirty-Forth IAS Annual Meeting, Phoenix, AZ, USA, 1999
[20] Ruba, M., Viorel, I.A., Szabó, L.: 'Modular stator switched reluctance motor for fault tolerant drive systems', *IET Electr. Power Appl.*, 2013, **7**, (3), pp. 159–169
[21] Akita, H., Nakahara, Y., Miyake, N., *et al.*: 'New core structure and manufacturing method for high efficiency of permanent magnet motors'. 38th IAS Annual Meeting on Conf. Record of the Industry Applications Conf., Salt Lake City, UT, USA, 2003
[22] Caricchi, F., Crescimbini, F., Honorati, O.: 'Modular, axial-flux, permanent-magnet motor for ship propulsion drives'. 1997 IEEE Int. Electric Machines and Drives Conf. Record, Milwaukee, WI, USA, 1997
[23] Drury, B.: 'Power semiconductor devices', in: '*Control techniques drives and controls handbook*' (IET, London, UK, 2009), pp. 109–169
[24] LEM, Datasheet: 'Current transducer HAIS 100-P', 2014
[25] Melexis, Application Note: 'Current sensors reference design guide', 2016
[26] Winterborne, D., Pickert, V.: 'Dynamic optimisation of switching points in switched reluctance drives'. IEEE 2nd Annual Southern Power Electronics Conf. (SPEC), Auckland, New Zealand, 2016
[27] Winterborne, D., Pickert, V.: 'Improving direct instantaneous torque control of switched reluctance machines with predictive flux constraints'. 8th IET Int. Conf. on Power Electronics, Machines and Drives, Glasgow, UK, 2016
[28] Gan, C., Wu, J., Sun, Q., *et al.*: 'Low-cost direct instantaneous torque control for switched reluctance motors with bus current detection under soft-chopping mode', *IET Power Electron.*, 2016, **9**, (3), pp. 482–490
[29] Sun, Q., Gan, C., Wu, J., *et al.*: 'OCTSF for torque ripple minimisation in SRMs', *IET Power Electron.*, 2016, **9**, (14), pp. 2741–2750